

Experimental investigation of existing R/C frames strengthened by high dissipation steel link elements

Apostolos A. Karalis^{*} and Kosmas C. Stylianidis^a

*Aristotle University of Thessaloniki, Faculty of Engineering, School of Civil Engineering
Laboratory of R/C and Masonry Structures, Thessaloniki, 54124, Greece*

(Received January 4, 2012, Revised April 18, 2013, Accepted April 25, 2013)

Abstract. This paper presents the results of an experimental program concerning the efficiency of a specific strengthening technique which utilizes a small steel link element connected to the R/C frame through bracing elements. Brittle types of failure, especially at the connections between steel and concrete elements, can be avoided by appropriate design of the local details. Five single storey one bay R/C frames scaled 1:3 were constructed according to older codes with substandard details. The first one was a typical bare reference frame. The other four were identical to the first one, strengthened by steel bracing elements. The behavior of the strengthened frames is described with respect to the reference bare frame. The concrete frames were constructed according to older code provisions by the use of smooth steel bars, low strength concrete, sparsely spaced stirrups and substandard details. The strengthening scheme aimed to the increase of both strength and deformation capacity of the original R/C frame. The inelastic deformations are purposely concentrated to a short steel link element connecting the steel bracing to the R/C frame. The results show that the steel link element can increase considerably the strength and the energy dissipation capacity of the frame.

Keywords: strengthening techniques; steel braced R/C frames; steel link; energy dissipation capacity

1. Introduction

The strengthening of existing old reinforced concrete (RC) buildings, mainly those with soft ground storey (pilotis), is a current necessity in seismic prone areas. It has been known for decades that infills upgrade drastically the seismic behavior of constructions. Many different types of infills were introduced for the strengthening of existing buildings, like reinforced or unreinforced masonry, reinforced concrete, precast reinforced concrete elements, aluminum or steel panels, steel bracings and steel link elements.

The scope of this work is the experimental investigation of a specific steel link element for the upgrading of existing buildings. Easy installation and replacement, low cost and low technological demand are the prim advantages of this technique.

Although the technique is not new, the limits of its application are not well investigated. Appropriate selection of shape, section and length of the link should lead to reasonable solutions.

^{*} Corresponding author, Civil Engineer MSc, Ph. D., e-mail: ap.karalis@gmail.com

^a Professor, e-mail: kcstyl@civil.auth.gr

As a lower limit, a significant improvement of the system must appear and, as an upper limit, the R/C frame must suffer a reasonable level of damage at the connections to the bracing system.

2. State of the art review

Maheri *et al.* (1997, 2003a, 2003b, 2003c) and Ghaffarzadeh *et al.* (2006) investigated experimentally the use of steel bracing in concrete frames. A steel truss for the strengthening of R/C frames was tested by Kunisue *et al.* (2000). Failure was observed at purposely used elastoplastic energy dampers. Test results show that the strength and the energy dissipation capacity can be significantly improved by the use of these dampers. A calculation method was also suggested for the estimation of the strength increase in strengthened R/C frames and satisfactory approximation between experimental and analytical results was observed. In tests performed by Perera *et al.* (2004) the strengthening of masonry infilled R/C frames was examined. In some frames the masonry was replaced by a system of two steel braces and significant improvement of the energy dissipation was observed. In an experimental work by Ishii *et al.* (2004), R/C frames were tested and various types of failure in R/C structural elements were observed. Frames were strengthened by the same system of two steel braces. Differences at the hysteresis loops were recorded for each type of specimen. The optimum response was observed in specimens with flexural failure at the columns. In R/C frames that were strengthened by the use of two steel braces, considerable increase of strength and energy dissipation capacity was observed. In that case, significant damage occurred at the ends of the top R/C beam. Tests on two full scale, 4 storey R/C frames were reported by Pinto *et al.* (2006). For the frame without any strengthening interventions, high vulnerability to seismic loads was observed. It was found that through the use of steel braces, the seismic response of the strengthened frame and the energy dissipation capacity are significantly improved. A full scale 3D two storey R/C frame was tested by Antonucci *et al.* (2006). Viscous dampers were used at the connection point of the top of the bracing system to the middle of the R/C beam. Three tests were performed by D'Aniello (2006) on an existing R/C building that was strengthened against seismic actions by the use of the same system of two steel braces. From the tests it was resulted that shear elements can be easily connected at the concrete and the steel elements and can also be easily replaced after an important seismic event. Mazzolani *et al.* (2004, 2006, 2009a, 2009b) investigated experimentally the use of various strengthening methods on existing full scaled two storey R/C frames, among others the use of steel bracing. Mehmet Baran *et al.* (2011) investigated experimentally and analytically the effectiveness of adding precast concrete infilled panels to existing R/C frames, already infilled by hollow bricks. Eight R/C frames, 1:3 scaled, were tested incorporating four different types of precast panels. The results showed that both strength and stiffness of the frame were significantly improved by the introduction of precast panels. Experimental results were compared with analytical approaches.

3. Description of the tests

3.1 Strengthening layout

As shown in Fig. 1, the bracing system is composed by two steel elements that are connected to each other at their top. At this point there is a steel plate on which the shear - flexural link element

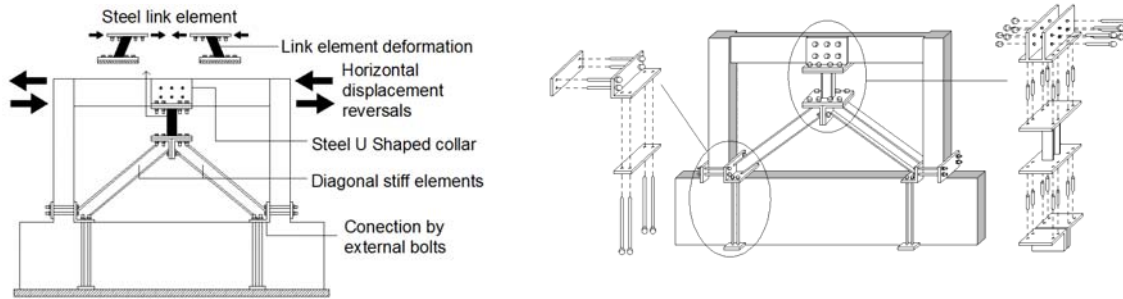


Fig. 1 Strengthening layout

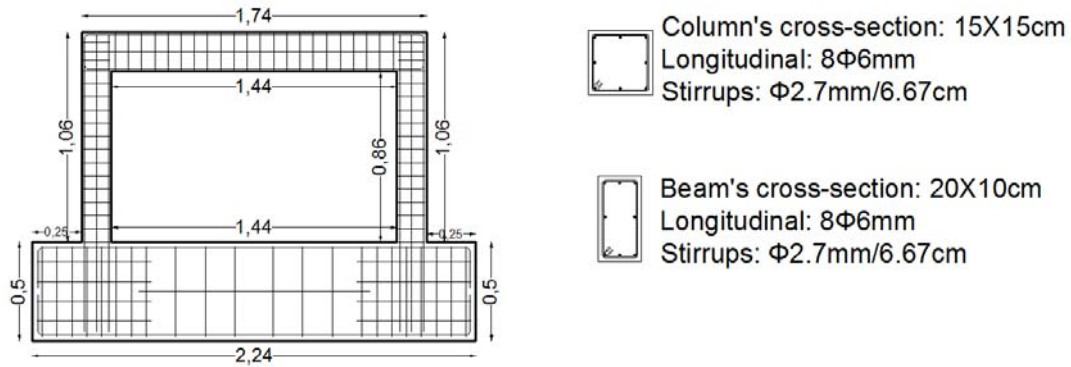


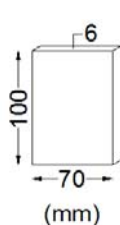
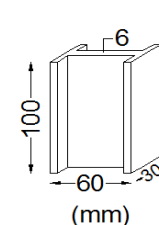
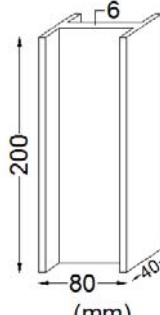
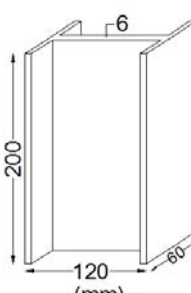
Fig. 2 Geometry (m) and reinforcement arrangement of the specimens

is welded. The top of the link element is connected to the midpoint of the beam through a steel U shaped collar which surrounds the beam. The collar element is connected to the top beam by six bolts from side to side of the beam. The diagonal elements of the bracing system are connected at their bottom with the column base and the foundation beam of the specimens by external bolts. The elements of the bracing system, the collar and the connections to the beams and the columns were not considered as parameters under investigation in the present study. Therefore they were oversized in order to avoid local failures at these elements. Consequently, the inelastic deformation of the strengthened specimens is expected to be concentrated mainly at the link element. This type of link elements are expected to significantly increase the strength and stiffness of the strengthened frame, but the most important advantage of these systems is the drastic reduction of the strength demand of the strengthened R/C elements against seismic actions due to their high energy dissipation capacity.

3.2 Specimens

The tests were carried out at the Laboratory of Concrete and Masonry Structures, Civil Engineering Department, Aristotle University of Thessaloniki. In this work results are given from the tests of five specimens constructed in 1:3 scale. The specimens represent a single storey one bay frame rigidly based on a strong foundation. The five R/C specimens are identical to each other. The geometry and the reinforcement arrangement of the specimens are shown in Fig. 2.

Table 1 Specimens names and geometry of the links

Specimens	F1	F2	F3	F4	F5
Link element	non	 (mm)	 (mm)	 (mm)	 (mm)

Although specimen F1 is a bare reference frame, the bracing system was placed as in the other four specimens, but without the link element. This layout was selected in order to ensure the same geometrical conditions for all the specimens concerning the effective height of the columns. In the other four specimens the bracing system was connected at the middle of the top beam by a steel link, different for each specimen (Table 1).

The percentage and the layout of the reinforcement, the steel and concrete quality and the type of reinforcement bars (smooth) were selected in order to simulate R/C frames that were constructed according to older codes using past construction techniques. The smooth steel bars for the longitudinal reinforcement had a yield to ultimate strength ratio $f_y/f_u = 442/517\text{MPa}$ (it was not possible to find lower strength smooth reinforcement bars 6mm in diameter) and for stirrups $f_y/f_u = 377/428\text{MPa}$. Low strength concrete was also used with $f_{ck} = 16\text{MPa}$. The reinforcement was arranged according to older code provisions without dense spacing at the critical areas of possible hinge regions at the ends of the concrete structural elements. The anchorage length of the steel bars was also small contrary to modern code provisions. The steel link elements had a yield to ultimate strength $f_y/f_u = 271/366\text{MPa}$ and geometrical dimensions shown in Table 1.

3.3 Experimental test setup

For the tests, the facilities of the Laboratory of Concrete and Masonry Structures, Aristotle University of Thessaloniki, were used (Fig. 3). The reaction frame consists of steel beams and columns connected to each other by prestressed bolts. One double acting actuator is connected at the top beam of the specimens applying horizontal displacement reversals. Another actuator can also be connected to the system to apply vertical axial loads on the columns through a top steel beam in a load control mode. This option was not activated for the present study.

The reaction frame is connected to the strong floor of the laboratory by the use of steel stoppers

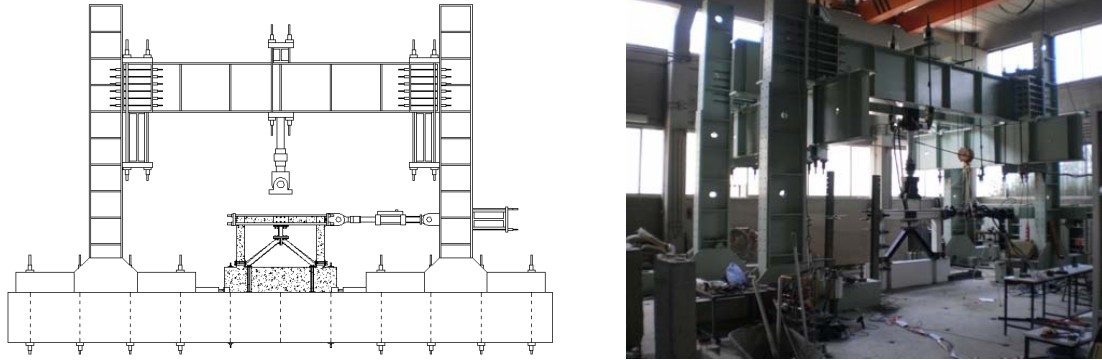


Fig. 3 Test setup

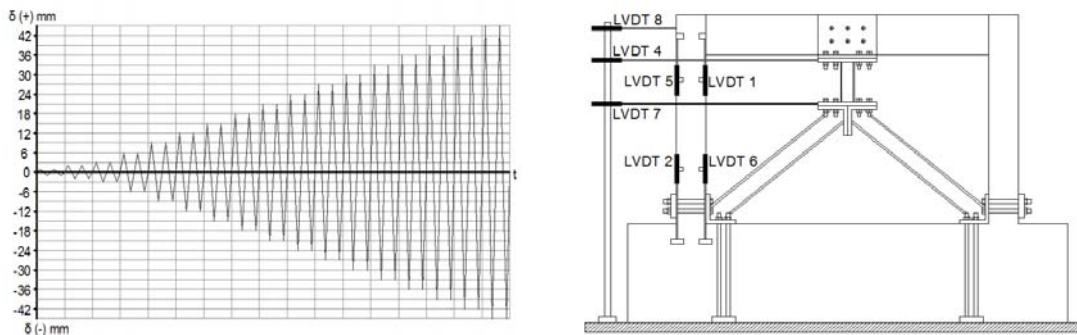


Fig. 4 Horizontal loading history and LVDT arrangement on the specimens

in combination with vertical prestressed anchored bolts. The test specimens were also connected to the floor by the same technique. It is worth mentioning that during the tests no slip was recorded between the specimens and the laboratory floor. The horizontal actuator was connected to the top of the specimens by a system of two stiff steel plates at the vertical outer sides of the beam - column joints, connected to each other by four long bolts. In order to provide rotational degree at the connection points, beyond the 3D rotational hinges of the actuator at the ends of its length, two more rotational hinges were provided between the steel plates and the two top beam - column joints of each specimen.

The horizontal loads were imposed in a displacement control mode. The displacement history is composed of 17 levels of displacement (Fig. 4). Due to the extended damage that developed, some tests were terminated earlier but the maximum strength had already been developed. For each displacement level, two full cycles were imposed.

The specimens were instrumented by the use of seven LVDTs. The layout of these instruments is shown in Fig. 4. LVDTs 1, 5, 2, 6 were used for the measurement of the shortening and the elongation of the outer fibers at the ends of the left column. LVDT 8 was used for the measurement of the top horizontal displacement of the specimen and was compared with the measurements of the internal LVDT of the horizontal actuator. LVDTs 4 and 7 were used for the measurement of the net horizontal displacement at the top and bottom ends of the steel link element. Some differences between instruments 8 and 4 occurred because the top collar of the shear - flexural element could not be completely horizontally restrained at the midpoint of the top

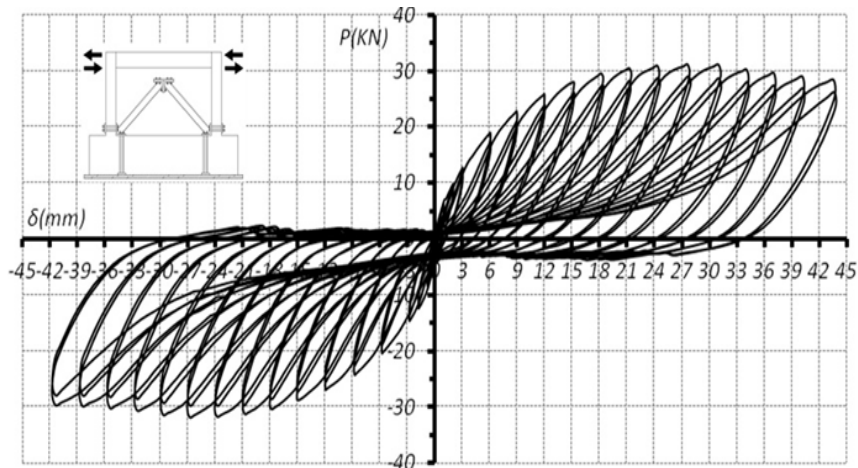


Fig. 5 Load - displacement (P - δ) curves of the frame F1

beam of the specimen. The measurements of the external LVDTs together with the measurements of the internal LVDT and load shell of the horizontal actuator were recorded through the digital controller. In the present work, only a small part of the experimental measurements and the postprocessed data are given due to limited available space.

4. Results

The discussion of the results is based mainly on the five characteristic diagrams given below for each specimen:

- Load - displacement ($P - \delta$) curves.
- Load - displacement ($P - \delta$) envelopes.
- Energy dissipation - displacement ($E - \delta$).
- Normalized energy dissipation - displacement ($E/2\delta - \delta$).
- Equivalent viscous damping - displacement ($\zeta - \delta$).

The displacement mentioned corresponds to the clear beam horizontal displacement (LVDT 8, Fig. 4). Note that, since the height of the specimens is almost 100cm, a displacement of 1cm corresponds almost to 1% storey drift.

4.1 Reference specimen F1

At early stages, during the first imposed cyclic displacements, horizontal or inclined cracks appeared, initially at the base and later at the top of the columns. The cracks at the base of the columns were formed just over the connection point of the bracing system to the columns (Figs. 10-11). Under high level of imposed displacements, plastic hinges were formed at the ends of the columns of the specimens. Although no specific measures were taken, such as local confinement, the strength of the specimen was slightly increased even for drifts close to 3% (Figs. 5-6). For higher levels of the imposed inelastic deformation, the strength degradation was very low. This

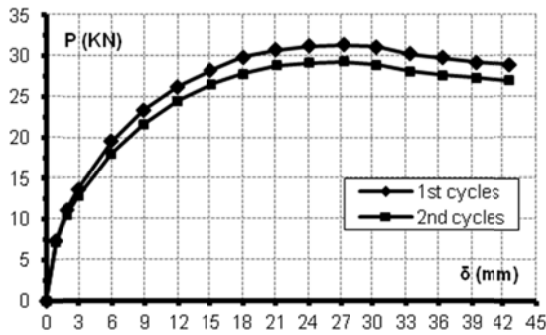


Fig. 6 Load - displacement ($P - \delta$) envelopes (F1)

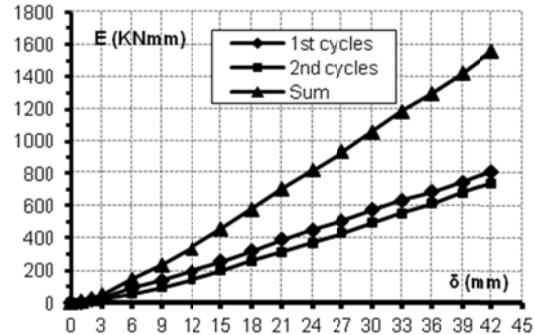


Fig. 7 Energy dissipation – displacement ($E - \delta$) envelopes (F1)

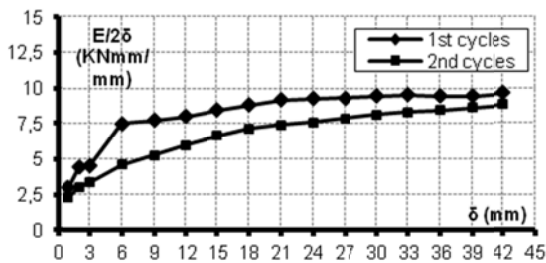


Fig. 8 Normalized energy dissipation - displacement ($E/2\delta - \delta$) envelopes (F1)

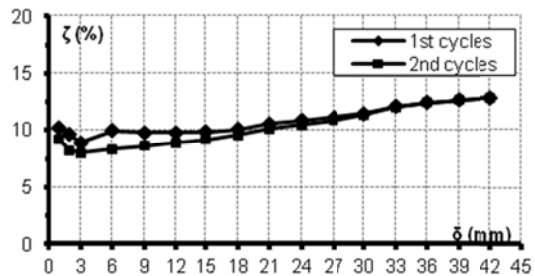


Fig. 9 Equivalent viscous damping - displacement ($\zeta - \delta$) envelopes (F1)

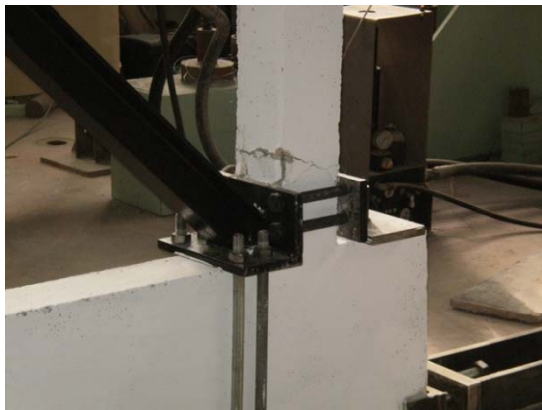


Fig. 10 Plastic hinge at the bottom of the column (F1)



Fig. 11 Specimen F1 at the end of the test

response is attributed to the prevailing flexural type of failure that was observed and measured during the tests. Taking into account the poor detailing of the specimen, although pinching is evident under reversals, the load - displacement hysteresis loops are rather rich. This is a characteristic of the relatively high energy dissipation capacity of the system (Fig. 7). During the second cycles at each displacement level, only a small reduction of the strength and the dissipation

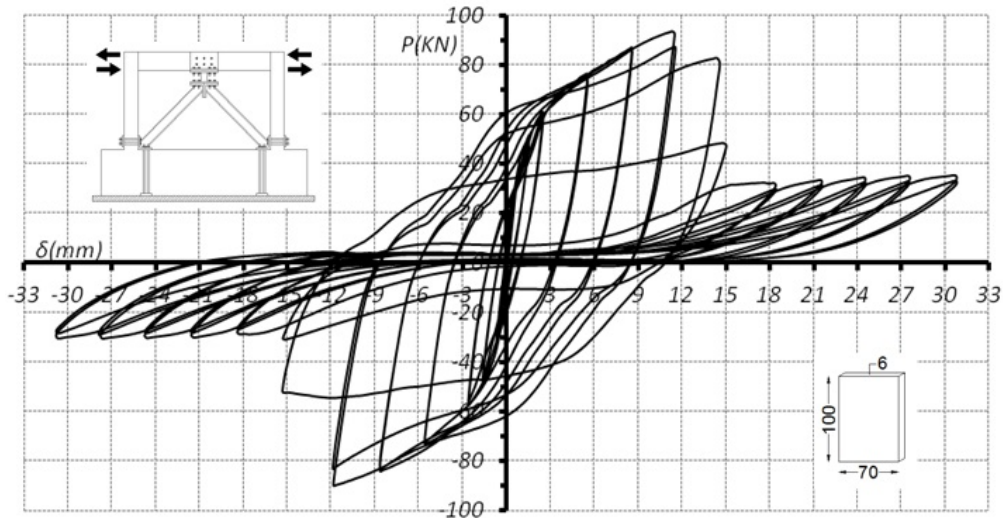


Fig. 12 Load - displacement (P - δ) curves of the frame F2

capacity is observed.

A rapid increase of the normalized energy dissipation is observed until the displacement of 6mm at the first cycles, and consequently the curve tends to stabilize at 10KNmm/mm in the maximum displacement 42mm. During the second cycles the curve is similar to the one of the first cycles but the values are lower (Fig. 8).

During the three firsts displacement levels, only a small reduction of the equivalent viscous damping is observed in both cycles and then, with a soft increase, stabilizes at the maximum value 13% (Fig. 9). From the displacement of 27mm and then the curve variation is exactly the same in both cycles.

4.2 Specimen F2

The steel link element significantly increased stiffness, strength and the energy dissipation capacity of the strengthened specimen F2, especially at the level of small imposed displacements. The welds did not show signs of failure.

This specimen presents an excellent behavior up to a drift of 12‰ (Figs. 12 and 13). The load carrying capacity is three times higher than that of the reference specimen F1, the hysteresis loops are very rich, no pinching is traced. The failure mode of the R/C frame is the same as in F1, since plastic hinges are formed again at the top and the bottom of the columns. The midpoint of the beam suffers some local cracking, but the cracking is not significant enough to alter the failure mode (Fig. 17). When the drift reaches about 12‰, the steel link element reveals a failure of a rather shear type, with a side to side horizontal crack at the top and the bottom ends (Fig. 18). After the complete detachment of the link element, the overall behavior, concerning strength and energy dissipation capacity, drops to the behavior of the reference specimen (Figs. 13-15). It is worth mentioning that no signs of unfavorable phenomena, such as considerable drop of strength during imposed reversals and pinching, are traced.

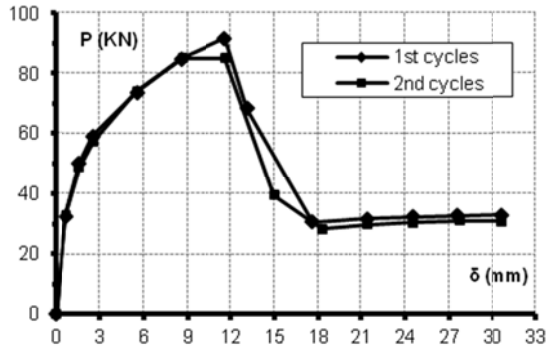


Fig. 13 Load - displacement ($P - \delta$) envelopes (F2)

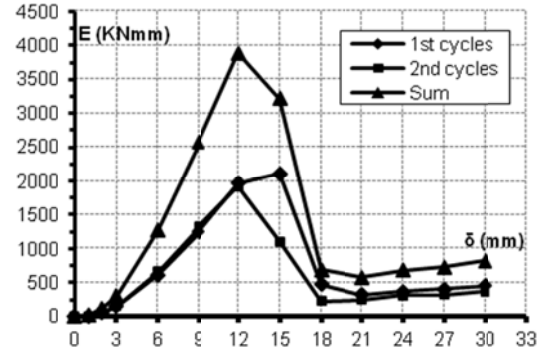


Fig. 14 Energy dissipation displacement ($E - \delta$) envelopes (F2)

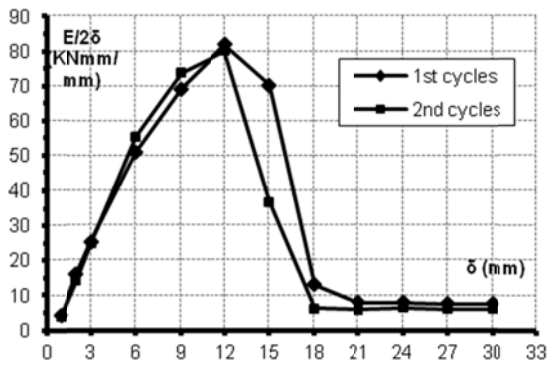


Fig. 15 Normalized energy dissipation - displacement ($E/2\delta - \delta$) envelopes (F2)

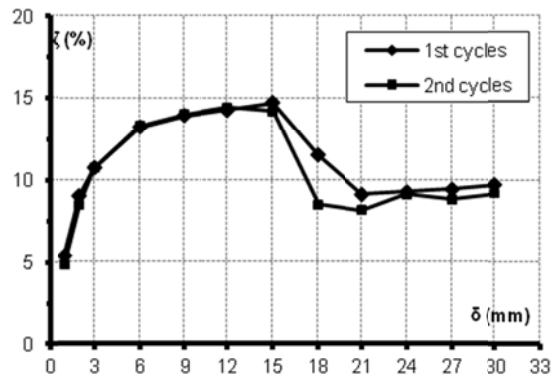


Fig. 16 Equivalent viscous damping - displacement ($\zeta - \delta$) envelopes (F2)



Fig. 17 Cracking at the middle of the beam (F2)

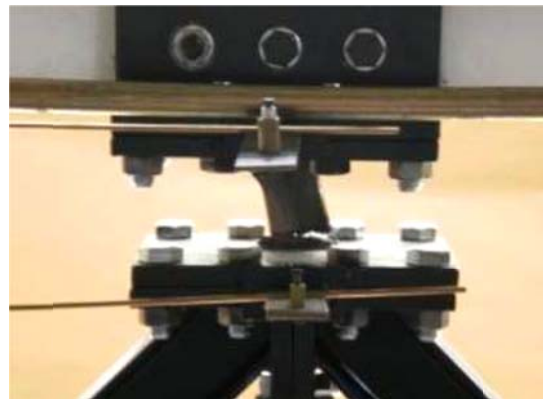


Fig. 18 Failure mode of the link element (F2)

A significant increase at the energy dissipation capacity is observed before the link element failure (drift 12%), which is about ten times higher than that of the reference specimen F1 (Figs. 14 and 15). The equivalent viscous damping presents an excellent behavior. When the drift reaches

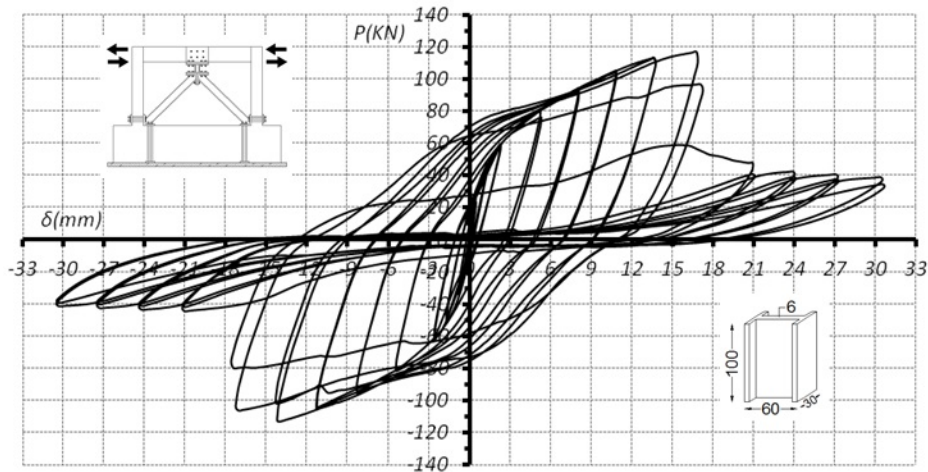


Fig. 19 Load - displacement (P - δ) curves of the frame F3

15‰, the equivalent viscous damping is almost 15% (Fig. 16). This percentage is very close to the perfect plastic behavior ($\zeta=1/2\pi=15,92\%$). After the failure of the link element this percentage drops to the behavior of the reference specimen.

4.3 Specimen F3

The failure mode of the R/C frame is the same as in the previous specimens, since plastic hinges are formed again at the top and the bottom of the columns. Once more time the midpoint of the beam suffers some local cracking (Fig. 24).

Specimen F3 reveals an even better behaviour compared to F2. Failure occurs at a drift of 18‰ (Figs. 19 and 20). The load carrying capacity is almost four times higher than that of the reference specimen F1, the hysteresis loops are also very rich, again no pinching is traced. At that level of drift the steel link element reveals a rather bending type of failure (Fig. 25). For a small amount of further displacements, the link element, although practically inactive, is not completely detached from the plates, still offering some strength and energy dissipation capacity before the full detachment occurs (Figs. 20-22). Again, no unfavorable phenomena are evident.

It is clear that the I shaped cross section in combination with the small length of the link element (100mm) resulted to a stronger and stiffer R/C frame compared to the specimens F1 and F2. A significant increase of the strength, the energy dissipation capacity and the equivalent viscous damping in both of cycles is observed, until the failure of the link element (drift 18‰) (Figs. 20-23). The flanges prevented the link element buckling and delayed the complete failure. The maximum strength of this appeared at a drift of 15‰. A small ductility increase is also observed due to the increase of failure drift at 18‰ compared to the specimen F2. After the failure of the link element, the overall behavior of the F3 specimen, in terms of strength and energy dissipation capacity, appeared to be similar to the behavior of the F1 frame.

The equivalent viscous damping presents similar behavior with that of the specimen F2. The maximum percentage (~14%) is observed before the link element failure (Fig. 23). The difference is that the maximum percentage is observed for a 18‰ drift, when the equivalent drift for the specimen F2 is 15‰.

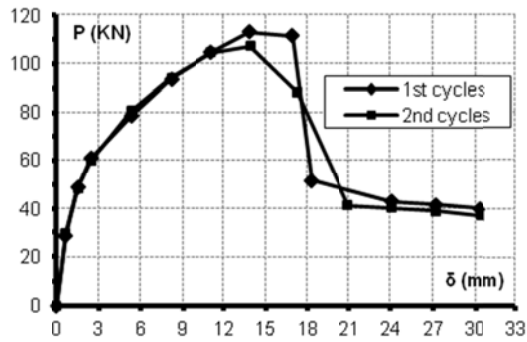


Fig. 20 Load - displacement ($P - \delta$) envelopes (F3)

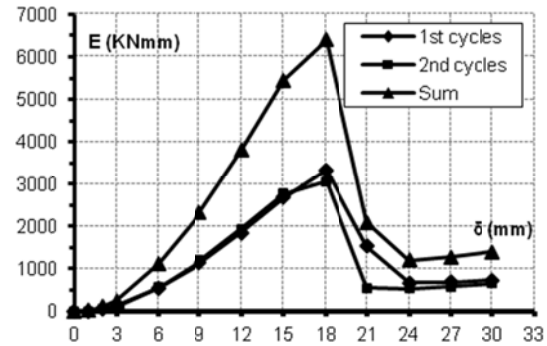


Fig. 21 Energy dissipation - displacement ($E - \delta$) envelopes (F3)

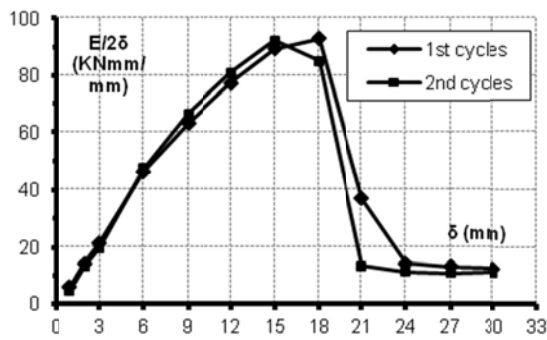


Fig. 22 Normalized energy dissipation - displacement ($E/2\delta - \delta$) envelopes (F3)

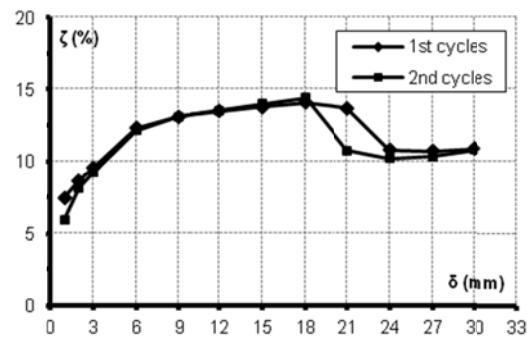


Fig. 23 Equivalent viscous damping - displacement ($\zeta - \delta$) envelopes (F3)



Fig. 24 Cracking at the middle of the beam (F3)



Fig. 25 Failure mode of the link element (F3)

4.4 Specimen F4

The dimensions of the cross-section of this link in combination with its longer length resulted

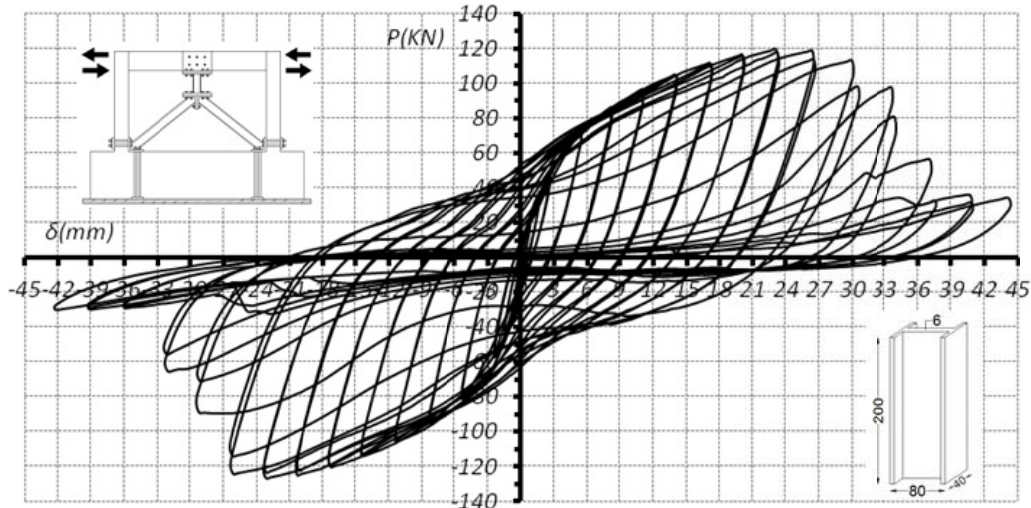


Fig. 26 Load - displacement (P-δ) curves of the frame F4

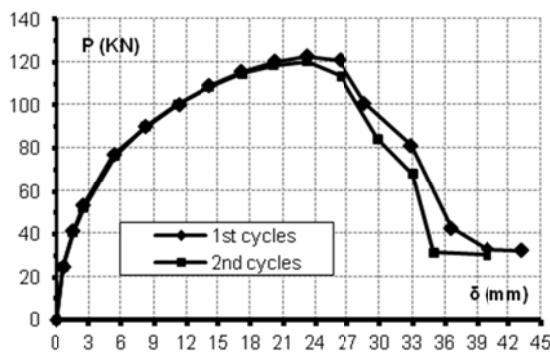


Fig. 27 Load - displacement (P - δ) envelopes (F4)

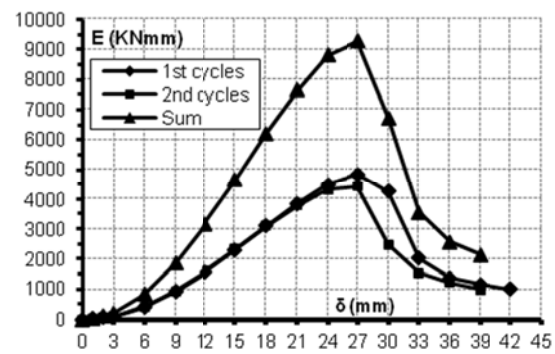


Fig. 28 Energy dissipation - displacement (E - δ) envelopes (F4)

to lower stiffness compared to the link of the specimen F3. However, the ultimate strength for this specimen is slightly higher than that of specimen F3. The main improvement for the present specimen is that the strength was increased without reduction until a drift of 27%, thus, improving the ductility of the strengthened frame (Figs. 26 and 27).

The failure of the link element started at a drift of 27% and was completed at a drift of 36%. After that point, the specimen dropped to the response of the unstrengthened specimen F1. This high ductility of the specimen is attributed to the higher rotational capacity of the link element. Due to the higher forces and the significant inelastic deformations that were developed, the U-shaped collar at the middle of the top beam caused local damage to the frame (Fig. 31). Moreover, the bending moment that developed at the mid-span of the beam due to the eccentricity of the horizontal force undertaken by the link, led to the development of high shear forces along the two parts of the beam and resulted to the bidiagonal shear cracks at the left and right parts of the top beam (Fig. 31). Plastic hinges were also formed at both ends of the columns.

The energy dissipation capacity (Figs. 28 and 29) was increased until the failure of the link

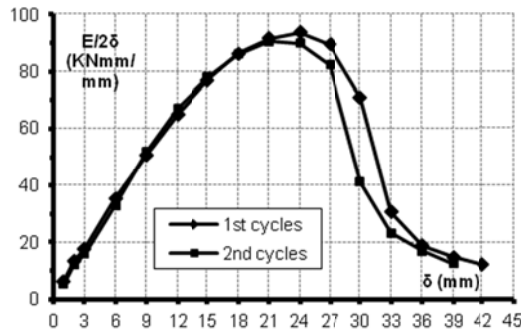


Fig. 29 Normalized energy dissipation - displacement ($E/2\delta - \delta$) envelopes (F4)

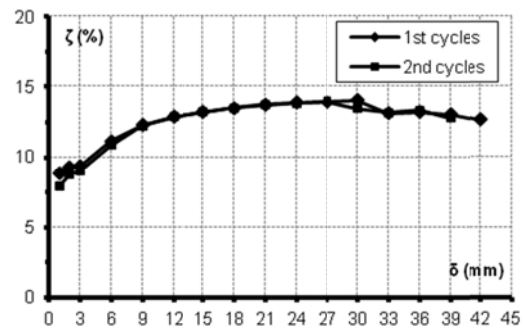


Fig. 30 Equivalent viscous damping - displacement ($\zeta - \delta$) envelopes (F4)

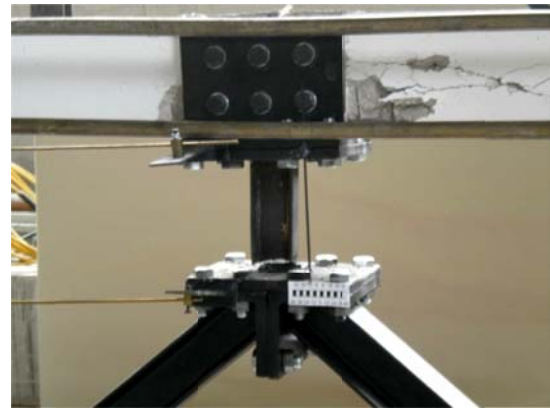


Fig. 31 Cracks at the middle of the top beam and failure mode of the link element (F4)

element. The equivalent viscous damping (Fig. 30) was also increased slightly until a drift close to 21%, remained constant without reduction until a drift of 27% and then dropped due to the link element failure.

4.5 Specimen F5

This specimen was strengthened by a high strength and stiffness link element. The scope for this choice was the investigation of the maximum response of the R/C frame under extreme strengthening intervention.

During the test the strength and the stiffness of the frame was quite higher compared to the other specimens. The maximum strength of 150kN was five times higher than the reference specimen (F1) and was observed at a drift of ~18% (Figs. 32 and 33).

At early stages, during the first imposed cyclic displacements horizontal cracks appeared initially at the base and the top of the columns. By imposing displacement reversals, the U-shaped jacket at the middle of the top beam progressively caused extended damage due to the relatively high force induced by the link element. At the end of the test, extended damage was observed in the R/C beam (Fig. 37). For this reason the test was terminated earlier in comparison to the other specimens. The link element suffered inelastic deformation but it was not detached from the plates.

The energy dissipation capacity was increased due to the rich hysteresis loops until the beam

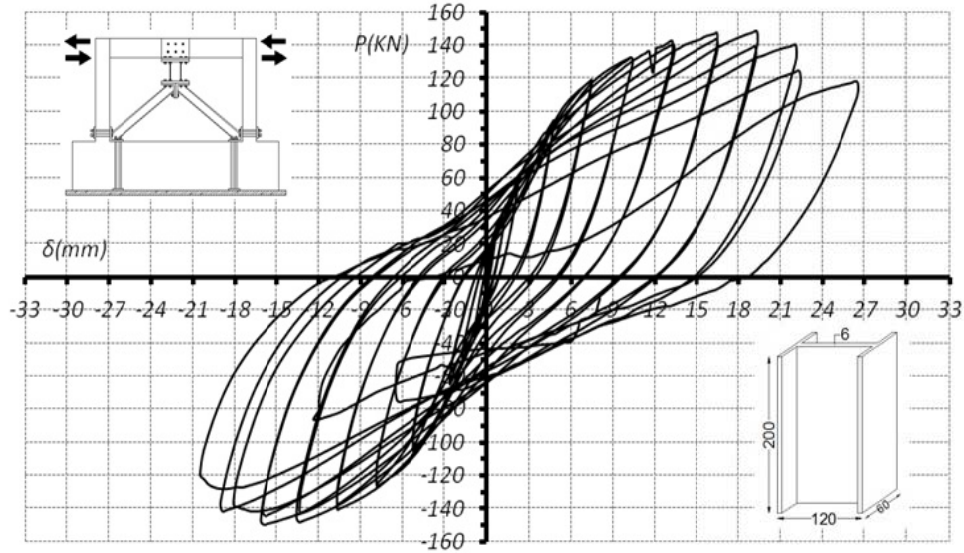


Fig. 32 Load - displacement ($P-\delta$) curves of the frame F5

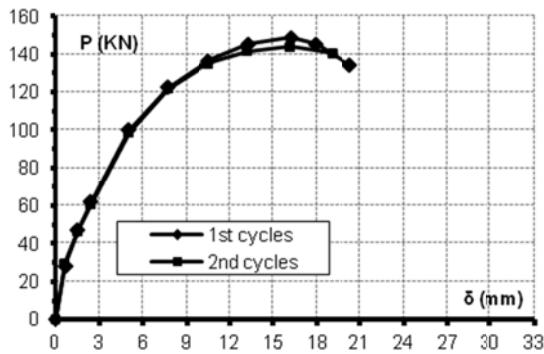


Fig. 33 Load - displacement ($P - \delta$) envelopes (F5)

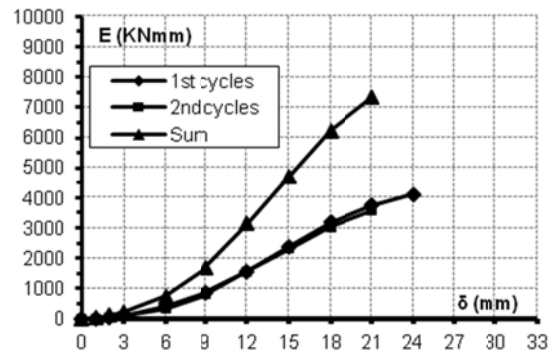


Fig. 34 Energy dissipation displacement ($E - \delta$) envelopes (F5)

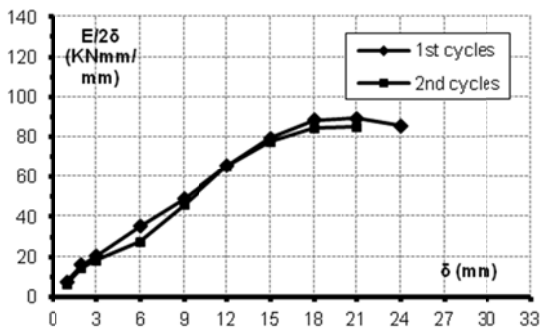


Fig. 35 Normalized energy dissipation – displacement ($E/2\delta - \delta$) envelopes (F5)

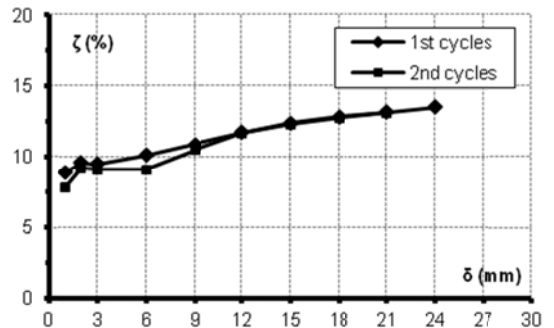


Fig. 36 Equivalent viscous damping - displacement ($\zeta - \delta$) envelopes (F5)



Fig. 37 Extended damage at the middle of the top beam (F5). The link did not fail

failure (Figs. 34 and 35). The equivalent viscous damping was also slightly increased until the end of the test with the maximum percentage at ~14% for drift of 24% (Fig. 36).

5. Comparisons between specimens

For the comparison of the overall behavior of the specimens, four diagrams are presented in Figs. 38-41, corresponding to first cycles only.

In Fig. 38 the loads are calculated as the mean of the absolute values of the positive and negative load carrying capacity at each displacement level. It is apparent that the strengthened specimens F2 and F3 are stiffer and stronger, about three and almost four times respectively in comparison to the reference specimen F1. The specimen F3 appears to behave better than the specimen F2 since it reveals higher strength and deformation capacity. The curve of specimen F4 is very close to the curves of specimens F2 and F3, before the failure of their link elements. The link element failure of specimen F4 was delayed due to the link element longer length. So the strength was increased even for drifts close to 21%. This type of link element increased drastically the ductility of the system. After the link element failure of specimens F2 - F4, the strength drops to the strength of the reference specimen F1. Specimen F5 presents a rapid increase of the strength but the higher forces due to the strong link element caused extended damage at the middle in the top beam and the strength of the frame drop earlier than in specimen F4.

From Figs. 39-40 it is evident that, at the displacement levels where the links are active, the strengthened specimens can dissipate energy about ten times than that of the reference specimen. Again, specimen F3 seems to behave better than the specimen F2. Specimen F4 dissipates more energy since its link element did not fail soon. The hysteresis loops for the specimen F5, despite its higher strength, are not richer. Again, after the link elements failure, the energy dissipation drops to the reference specimen behavior. In Fig. 40 the normalized energy dissipation shows that the maximum value was almost the same for all strengthened specimens and appeared just before the link element failure.

The equivalent viscous damping (Fig. 41) for the reference specimen (F1) presents an almost linear increase from 8% to 13% during the test. It is clear that all the curves of the strengthened specimens tend to reach the perfect plastic behavior ($1/2\pi=15,92\%$) at early stages of displacement.

It is significant to observe that equivalent viscous damping of the strengthened specimens is about 50% greater than that of the reference frame in the range of accepted drifts 5 to 15%. For one more time, the curves of the strengthened specimens after their link element failure drop to the reference specimen curve.

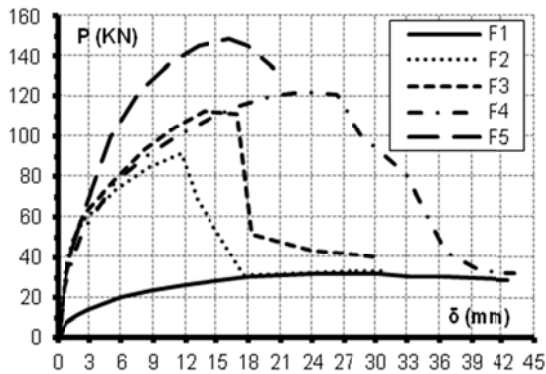


Fig. 38 Load - displacement ($P - \delta$) envelopes (F1-F5)

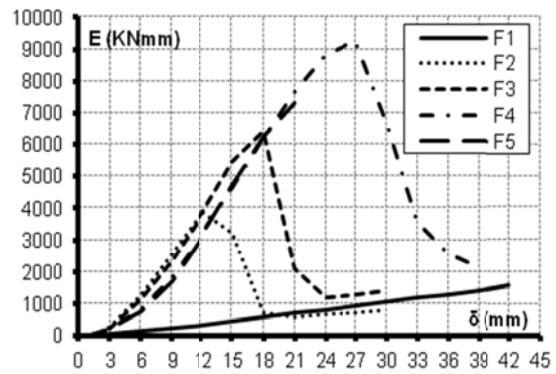


Fig. 39 Energy dissipation - displacement ($E - \delta$) envelopes (F1-F5)

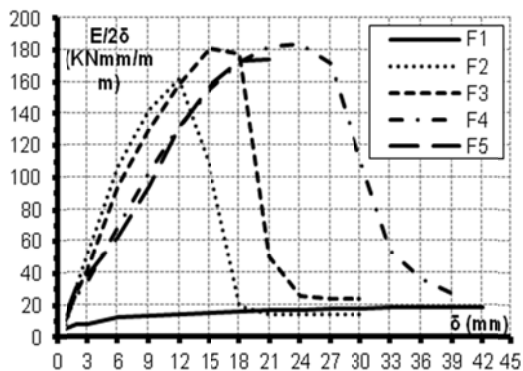


Fig. 40 Normalized energy dissipation - displacement ($E/2\delta - \delta$) envelopes (F1-F5)

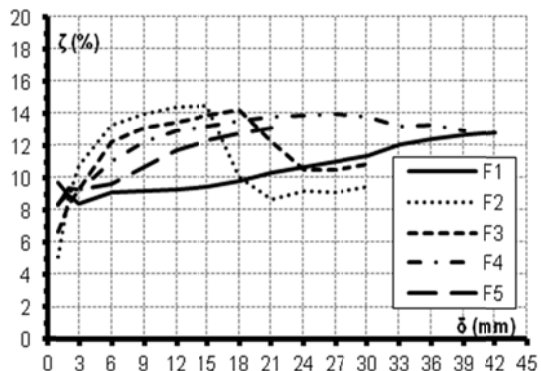


Fig. 41 Equivalent viscous damping - displacement ($\zeta - \delta$) envelopes (F1-F5)

6. Conclusions

The main conclusions from the observed and the recorded response of the strengthened specimens are the following:

- The use of steel link elements for the improvement of the seismic response of existing buildings is a low cost, low technology level and fully reversible method.
- In the case of open ground floors, the local application of the technique practically causes no inconvenience for the users of the building.
- Under excessive seismic conditions the damage of the bracing system is expected to concentrate to the steel links only, which can easily be replaced.

- Steel link elements can increase considerably the stiffness and the strength but they mainly increase the energy dissipation capacity.
- By a thorough selection of the geometrical dimensions, the shape and the material quality of the steel link elements, the unfavorable early local failure at the middle of the top beam of an existing R/C frame can be prevented. There is a need for careful design of the connection of the steel link element to the R/C top beam.
- The influence of the axial force on the columns is significant and is under experimental investigation.
- Further experimental research effort is under way to improve the advantages of steel link elements for the strengthening of existing R/C frames.
- Analytical research to simulate the experiments has already started and the results are encouraging.

Acknowledgments

The work presented here is part of a broader program partially sponsored by the Greek Earthquake Planning and Protection Organization, the contribution of which is gratefully acknowledged.

References

- Antonucci, R., Balducci, F., Bartera, F., Castellano, G. and Chaudat, T. (2006), "Shaking table tests on RC frame braced with fluid viscous dampers", *1st European Conference of Earthquake Engineering and Seismology*, Geneva, # 650.
- Baran, M., Susoy, M. and Tankut, T. (2011), "Strengthening of deficient RC frames with high strength concrete panels: an experimental study", *Struct. Eng.Mech.*, **37**(2), 177-196.
- D'Aniello, M. (2006), "Seismic upgrading of RC structure by steel eccentric bracing (an experimental and numerical study)", *Pollack Periodica, An international journal for Engineering and information Sciences*, **1**(2), 17-32.
- Ghaffarzadeh, H. and Maheri, M.R. (2006), "Mechanical Compression release device in steel bracing system for retrofitting RC frames", *Earthq. Eng. Eng.Vib.*, **5**(1), 151-158.
- Ishii, T., Mukai, T., Kitamura, H., Shimizu, T., Fujisawa, K. and Ishida, Y. (2004), "Seismic retrofit for existing r/c building using energy dissipative braces", *13th World Conference on Earthquake Engineering*, Canada, # 1209.
- Kunisue, A., Koshika, N., Kurokawa, Y., Suzuki, N., Agami, J. and Sakamoto, M. (2000), "Retrofitting method of existing reinforced concrete buildings using elasto-plastic steel dampers", *12th World Conference on Earthquake Engineering*, New Zealand, #648.
- Maheri, M.R. and Sahebi, A. (1997), "Use of steel bracing in reinforced concrete frames", *Eng. Struct.*, **19**(12), 1018-1024.
- Maheri, M.R. and Akbari, R. (2003a), "Seismic behaviour factor, R , for steel X-braced and knee-braced RC buildings", *Eng. Struct.*, **25**, 1505-1513.
- Maheri, M.R. and Hadjipour, A. (2003b), "Experimental investigation and design of steel brace connection to RC frame", *Eng. Struct.*, **25**, 1707-1714.
- Maheri, M.R., Kousari, R. and Razazan, M. (2003c), "Pushover tests on steel X-braced and knee-braced RC frames", *Eng. Struct.*, **25**, 1697-1705.
- Mazzolani, F., Della Corte, G. and Faggiano, B. (2004), "Seismic upgrading of RC buildings by means of

- advanced techniques: The ILVA-IDEM project”, *13th World Conference on Earthquake Engineering*, Vancouver, B.C., Canada, August 1-6, #2703.
- Mazzolani, F. (2006), “Seismic upgrading of RC buildings by advanced techniques”, *The ILVA-IDEM Research Project, Polimetrica, International Scientific Publisher*.
- Mazzolani, F. (2009a), “Steel bracing systems for the seismic upgrading of RC structures”, *Steel Construct.*, **2**(4), 235-242.
- Mazzolani, F., Dell a Corte, G. and D’ Aniello, M. (2009b), “Experimental analysis of steel dissipative bracing systems for seismic upgrading”, *J. Civil Eng.Manag.*, **15**(1), 7-19.
- Perera R., Gomez, S. and Alarcon, E. (2004), “Experimental and analytical study of masonry infill reinforced concrete frames retrofitted with steel braces”, *J. Struct. Eng.*, **130**(12), 2032-2039.
- Pinto, A. and Taucer, F. (2006), “Assessment and retrofit of full scale models of existing RC frames”, *Advances in Earthquake Engineering for Urban Risk Reduction*, pp 353-367.